Available online at www.sciencedirect.com
SCIENCE DIRECT®
Nuclear Instruments and Methods in Physics Research A 514 (2003) 215–223
NUCLEAR INSTRUMENTS & METHODS IN PHYSICS RESEARCH Section A
www.elsevier.com/locate/nima

Initial studies on proton computed tomography using a silicon strip detector telescope

L. Johnson[a], B. Keeney[a], G. Ross[a], H.F.-W. Sadrozinski[a,*], A. Seiden[a], D.C. Williams[a], L. Zhang[a], V. Bashkirov[b], R.W. Schulte[b], K. Shahnazi[b]

[a] *Santa Cruz Institute for Particle Physics, University of California Santa Cruz, Santa Cruz, CA 95064, USA*
[b] *Loma Linda University Medical Center, Loma Linda, CA 92354, USA*

Abstract

We report initial results of a feasibility study of Proton Computed Tomography and Proton Transmission Radiography for applications in proton therapy treatment planning and patient positioning. The aim of the study is to explore experimentally if PCT, which is based on the measurement of the specific energy loss of protons traversing tissues of different density, may be preferred to X-ray Computed Tomography and X-ray radiography, which are presently used for radiation treatment planning and patient positioning in proton treatment centers.

We present first data from proton transmission studies through a hollow aluminum cylinder taken with a telescope of silicon detectors with very high spatial and good energy resolution. In addition, we report the results of GEANT4 simulations of proton transport through the same object, which show good agreement with experimental results and explain the observed features of the proton transmission image.

PACS: 87.58.−b

Keywords: Proton CT; Silicon detectors

1. Introduction

Proton radiation therapy is a precise form of radiation therapy. Avoidance of damage to critical normal tissues and prevention of geographical tumor misses require accurate knowledge of the dose delivered to the patient and verification of the correct patient position with respect to the proton beam. In existing proton treatment centers dose calculations are performed based on X-ray Computed Tomography (CT) and the patient is positioned with X-ray radiographs [1].

Computed Tomography makes use of the differential attenuation of photons, which mainly depends on the atomic number Z of the materials. Stacked 2D maps of linear X-ray attenuation, representing a faithful reconstruction of the patient's anatomy, are generated by numerically solving a set of coupled linear equations. However, the use of X-ray CT images for proton treatment planning ignores fundamental differences in physical interaction processes between photons and protons and is, therefore, potentially inaccurate.

*Corresponding author. Tel.: +1-831-459-4670; fax: +1-831-459-5777.
E-mail address: hartmut@scipp.ucsc.edu (H.F.-W. Sadrozinski).

0168-9002/$ - see front matter © 2003 Elsevier B.V. All rights reserved.
doi:10.1016/j.nima.2003.08.108

Further, X-ray radiographs mainly depict patients' skeletal structures and rarely show the tumor itself. Ideally, one would image the patient directly with protons, for example, by measuring their energy loss after traversing the patient [2]. This method has the potential to significantly improve the accuracy of proton radiation therapy treatment planning and the alignment of the target volume with the proton beam.

We recently have begun to investigate the feasibility of Proton Beam Computed Tomography (PCT) and Proton Transmission Radiography (PTR). Our initial investigation consists of three steps:

- Exploratory study of PTR using a simple phantom in front of two silicon detectors, and comparison of the measurements with GEANT4 Monte Carlo (MC) simulations (subject of this paper).
- Theoretical study of PTR using the GEANT4 MC simulation package to investigate the influence of multiple Coulomb scattering (MCS) and energy straggling on image resolution and contrast.
- Development of 3D-PCT reconstruction algorithms to be tested with phantoms and small animals mounted on a turntable to reconstruct a 3D density map of these objects.

In this paper, we will briefly review the basic physical processes of the proton energy loss in matter, followed by a description of the present experimental setup and the performance of proton energy measurements with the silicon detectors used for this experiment. We then describe the data obtained with PTR of a simple object and compare them with the results of MC simulations, followed by conclusions and outlook on the next steps of our program.

2. Proton energy loss in matter

Unlike diagnostic X-rays, which interact with the image object mainly through the Compton scattering process, protons with energies used in therapeutic applications (70–250 MeV) lose energy mainly through inelastic collisions with atomic electrons as described by the Bethe–Bloch equation [3].

The specific energy loss, which is defined as the rate of energy loss per unit length of particle trajectory l, is proportional to the density ρ and the average ratio Z/A of atomic number and atomic weight of the traversed medium. It is useful to evaluate the energy loss as a function of the density weighted track length $x = \rho * l$, which is mass per unit area with the units g/cm^2. As a function of this variable x, the energy loss is called "stopping power" $\mathrm{d}E/\mathrm{d}x$, and represents a function with only a weak dependence on the material traversed, i.e. $\mathrm{d}E/\mathrm{d}x \sim Z/A$ [4]. Data on the proton stopping power in many materials are available on the NIST web site [5].

Since for most human tissues Z/A is relatively constant, the local energy loss depends on the local density of the object. The energy loss of an individual proton traversing an object is thus a measure of the line integral of the local proton energy losses along the proton path l:

$$\Delta E = \int_x \frac{\mathrm{d}E}{\mathrm{d}x}\,\mathrm{d}x = \int_l \rho(\mathbf{r}) \left(\frac{\mathrm{d}E}{\mathrm{d}x}(\mathbf{r})\right) \mathrm{d}l \qquad (1)$$

where $\mathbf{r}$ represents the spatial location within the object. For the relatively large proton energies ($\approx$100 MeV) used in PCT and PTR the stopping power has a sufficiently weak energy dependence so that it will not depend on the detailed local density distribution and the resulting varying local energy loss. Thus, measurement of the energy loss of protons traversing an object is a good measure of the projected integral density along the proton trajectories, which can be used to reconstruct a 3D density map of the object.

3. Experimental setup

Our approach to PRT and PCT is based on state-of-the-art silicon strip detectors (SSDs), which measure the energy and position of individual protons. The SSDs provide information about the position of the particle track from the strip-hit information, and about the particle's energy via the energy deposition measured in each

detector. This system, described in greater detail in Ref. [6], permits measurements of the proton position to about 50 μm and determination of the energy of protons in the 20–300 MeV range. The proton energy is derived from the specific energy deposition in each SSD using the time over threshold (TOT) signal as described below.

The SSDs used for our experiments, manufactured by Hamamatsu Photonics HPK, were originally developed for the Gamma-Ray Large Area Space Telescope (GLAST) [7]. The single-sided, AC coupled p-on-n detectors are manufactured from high-resistivity wafers of 400 μm thickness, with a pitch of 194 μm, and outer dimensions of 6.4 cm × 6.4 cm. A total of 320 strips are read out per SSD plane, with the SSD biased at about 100 V. Fig. 1 shows one of the two modules used for our experiment.

The setup for our initial experiment, schematically shown in Fig. 2, was installed on the research beam line of the medical proton synchrotron at Loma Linda University Medical Center [1]. A monochromatic 250 MeV proton beam was degraded by a 25.4 cm thick (approximately cube-shaped) wax block ($\rho = 0.926\ \mathrm{g/cm^2}$) to a mean energy of about 130 MeV.After a drift distance of 25 cm, the beam encountered the image object, a 5.0 cm long hollow aluminum cylinder ($\rho = 2.7\ \mathrm{g/cm^3}$), of outer diameter OD = 3.0 cm, and inner diameter ID = 0.68 cm. Behind the object, protons were individually detected by two silicon detector modules, each consisting of a pair of single-sided SSDs with strips oriented at right angle to each other. These detectors, located immediately behind and 27 cm downstream of the object, served to measure the spatial coordinates, x and y, and energy of the protons that either passed by or traversed the object.

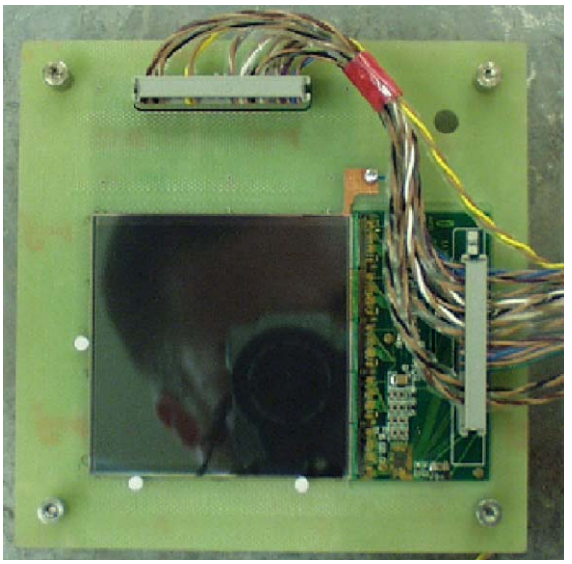

Fig. 1. One of the two silicon modules used in the PTR experiment. The 6.4 cm × 6.4 cm SSD and the MCM with five GTFE and one GTRC ASICs are visible. Alignment of the SSDs on the two sides to each other was accomplished by the Delrin posts and precision cutting of the SSD to 20 μm.

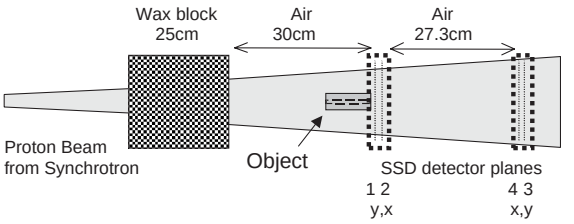

Fig. 2. Experimental setup of the PTR experiment. The energy of the proton beam at the exit of the synchrotron is 250 MeV, and the expected mean energy after the wax block is 130 MeV.

4. Energy measurement

A low-noise, low-power, front-end ASIC, the GLAST Tracker Front End (GTFE), developed for the GLAST mission, is used for the readout of the fast silicon detector signals [8]. At 1.3 μs shaping time, the SSDs have very large signal-to-noise (> 40), and thus very few extra noise hits. The five GTFEs on each silicon detector are read out via a digital controller ASIC, the GLAST Tracker Readout Controller (GTRC), into the data acquisition computer. The GTFE is a binary chip with a threshold settable individually for every channel and a fast output of the TOT, which is used for energy measurement. Self-triggering is accomplished through an OR of the TOT of all channels on one detector. The GTRC allows digitization of the TOT, yielding a measurement of the input charge via the pulse width, i.e., the TOT signal, over a large dynamic range. One feature of the selected ASIC is that only one TOT

value is returned per SSD even if more then one strip is hit. The TOT value is the OR of all pulse widths. Thus, to achieve good energy resolution, events with only one hit per SSD have to be selected such that there is no appreciable charge sharing between strips. The TOT values for hits next to any non-functional strips also have to be eliminated because the extent of charge sharing is unknown in this case.

The electronic calibration of the ASICs demonstrated a linear dependence of the TOT on the charge input up to a duration of 100 μs, at which point TOT saturation sets in. This translates into valuable energy measurements up to an input charge of 100 fC, which corresponds to the charge deposited by 17 MeV protons in 400 μm thick Si. We have tested the energy measurement performance of the SSD–TOT system with proton beams of energies between 5 and 250 MeV and recorded the TOT spectra [6]. Fig. 3a shows the mean TOT derived from these spectra as a function of the average incident proton energy together with the expected TOT values. The latter were determined from the calculated energy loss in silicon and the electronic calibration. The root mean square (RMS) values of the TOT data are shown as error bars. There is excellent agreement between measured and predicted TOT values over the entire energy range from 17 to 250 MeV. As expected, the TOT values saturate below 17 MeV. Although not tested experimentally, one can expect that protons with less than 2.3 MeV energy will also produce a measurable TOT signal (Fig. 3a).

It is clear from Fig. 3a that there is less energy discrimination for higher proton energies due to the reduced dependence of the energy loss on primary proton energy. We can derive an estimate of the energy resolution of the system, σ_E from the observed RMS of the TOT, σ_{TOT}, and the derivative of the TOT vs. energy curve Fig 3a:

$$\sigma_E = \sigma_{\mathrm{TOT}} \Big/ \frac{\partial \mathrm{TOT}}{\partial E} \tag{2}$$

Using the expected and experimentally confirmed TOT vs. energy curve, we find that the energy resolution σ_E/E below 40 MeV is on the order of 15% and increases to about 25% at 250 MeV (Fig. 3b).

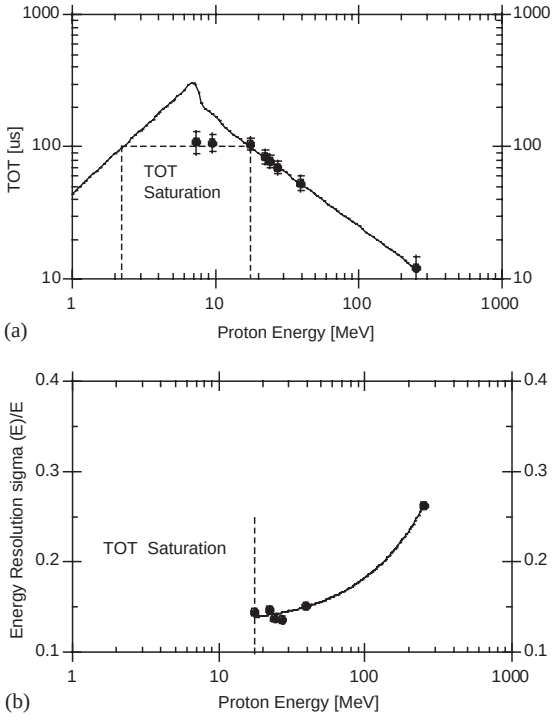

Fig. 3. Relationship between proton energy and TOT signal. The discrete points and error bars correspond to the mean and RMS values of the measured TOT spectra, respectively. The line represents the expected relationship between mean TOT and proton energy and was calculated based on the predicted energy loss of protons in 400 mm thick silicon detectors [5], the mean energy required for creating an electron–hole pair in silicon (3.6 eV) and the electronic calibration of the SSD. The slope discontinuity at low proton energy occurs because protons are stopped inside the silicon detector when their range in silicon is less than 400 μm. The area of saturation of the TOT signal is indicated. (b) Relative energy resolution $\sigma(E)/E$ of the silicon detectors using the TOT signal. The discrete points were calculated according to Eq. (2) using the RMS values of the TOT measurements as estimates for σ_{TOT} and the relationship between the TOT signal and energy (Fig. 3a) to derive $\partial \mathrm{TOT}/\partial E$. The line is based on the assumption of a linear relationship between energy resolution and proton energy.

5. Experimental results

The event data collected in our experiment comprized (x- and y-) hit positions and TOT values of the four silicon planes. As explained in the previous section, unambiguous energy measurements can only be performed on planes with

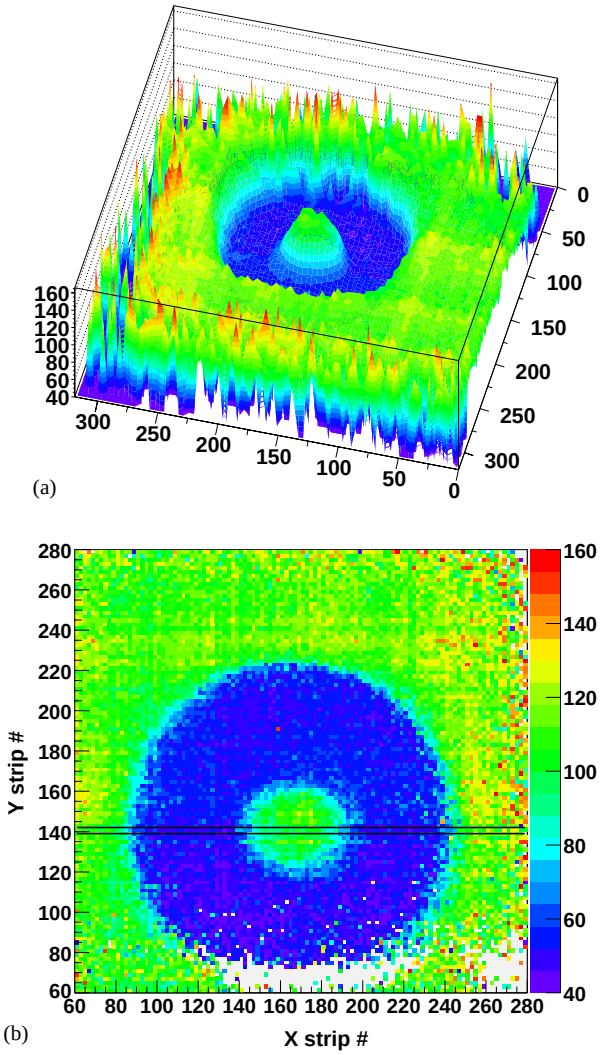

Fig. 4. Spatial distribution of the average energy of protons hitting all four SSD planes with single-strip resolution at the level of the upstream SSD module. (b) Energy projection onto the SSD plane after averaging over pixels of four by four strips. The image of the object can be clearly seen. The horizontal lines in Fig. 4b indicate the approximate location of the slice of Figs. 5 and 6.

exactly one hit. For simplicity, we selected only events with exactly one hit in all four silicon planes and averaged the energies derived from the TOT measurements of two adjacent detector planes. Proton transmission images were calculated for each SSD module by averaging the proton energy over a large number ($\sim 10^6$) of individual events, and displayed as 2D maps of proton energy versus the x- and y-strip positions in the respective SSD module. It was found that the image measured with the downstream module (SSD planes 3 and 4) showed almost no object features, which can be explained by the effect of multiple scattering (see Section 6). The 3D plot in Fig. 4a shows the spatial distribution of average energy in the upstream module with single strip resolution (pixel size approximately $0.2 \times 0.2\,\mathrm{mm}^2$), while the gray-scaled projection in Fig. 4b displays the same image after the proton energy was averaged over pixels of four by four strips (pixel size

approximately $0.8 \times 0.8\,mm^2$). The image of the phantom projection is clearly seen in the spatial energy distribution. Note that the depth of the structure in Fig. 4a is directly proportional to the energy loss in the aluminum object and thus is proportional to the product of its length and density. Fig. 4 thus demonstrates the principle possibility of image formation based on the spatial measurement of proton energy loss behind the image object. Future work will be devoted to improve the accuracy and range of the energy loss measurements.

We further analyzed the transmission image of Fig. 4 by selecting a 4 y-strip wide "slice" through the center of the cylinder ($139 \leqslant y \leqslant 142$, as indicated in Fig. 4b), containing pixels of four-by-four strips. Depending on their location, the number of proton events per pixel varied between 100 and 500 protons, owing to the non-uniformity of the beam. The average proton energy as a function of the average x-strip number of each pixel is shown in Fig. 5. The position of the object relative to the SSD is indicated by vertical lines. The following observations can be made:

- The observed energy profile agrees well with the borders of the object.
- The mean energy of the protons inside the central hole of the object is lower than that of protons outside the object.
- The margins of the energy profile are "fuzzy", i.e., not vertical.

6. GEANT4 simulations

To better understand the features of the proton transmission images presented in Section 5, we performed simulations with the Monte Carlo code GEANT4. The GEANT4 code has proved its ability to faithfully simulate the interaction of protons down to low energy [9]. In the future, the code will be used to define cuts on the data to optimize spatial resolution and contrast of the proton images.

Fig. 6a shows the simulated energy profile in the x and y silicon planes close to the object. The location of the profile corresponds to that in Fig. 5. The simulated profile agrees well with the measured outline of the object and with the measured energy profile. Compared to the simulated energy, the measured mean energy of protons not traversing the object is about 10% smaller.

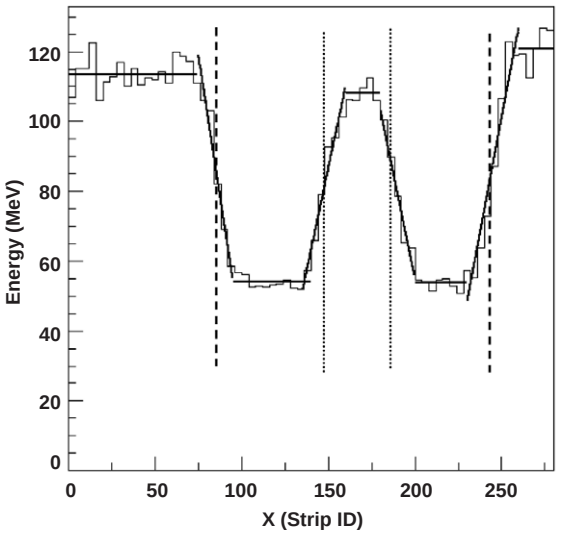

Fig. 5. Average energy profile in the slice through the center of the object, as indicated in Fig. 4b. The solid lines are drawn by eye. The dashed (dotted) lines show the approximate location of the outer (inner) walls of the object with respect to the SSD.

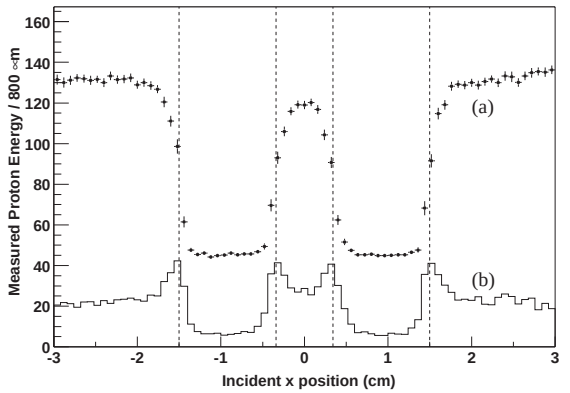

Fig. 6. (*upper half of illustration*) Monte Carlo simulation of the average energy profile of the first SSD module in a four-strip wide slice through the center of the object. The dashed vertical lines indicate the relative position of the object with respect to the SSD plane. (b) (*lower half*) RMS deviation of the proton energy. Note the increase in the RMS at the interfaces between object and air.

Given that our preliminary calibration procedure of the ASIC response is expected to be accurate to 15%, this is within our expectation. Work in progress will decrease this discrepancy of the overall energy scale. The mean simulated energy of protons transmitted through the hole is about 10% lower than that for protons passing outside the object, as observed in the experimental data (Fig. 5). Furthermore, in agreement with the measured energy profile, both the inner and outer margins of the energy-loss profile are fuzzy.

These image features can be explained by "migration" of protons from the object into the surrounding space due to multiple Coulomb scattering and the divergence of the degraded proton beam. This assumption is supported by the distribution of the energy spread, shown in Fig. 6b, which is larger at the interfaces between the object and the surrounding air, indicating a mixture of protons with and without energy loss in this region. It can be assumed that the protons with lower energies entered the object trough the front surface and exited through the sides.

Fig. 7 demonstrates the effect of the distance between the image plane and the object. Here, the simulated energy loss distributions, rather than the energy distributions, are shown for the two modules. As indicated in Fig. 3a, smaller proton energies correspond to a larger energy loss. Compared to the image produced by the upstream detector planes, the object image in the downstream detector planes is almost completely washed out. This shows that the proton tracks have a relatively wide angular distribution.

Further evidence for proton migration is given in Fig. 8, which shows the hit-number (occupancy) profile of the same slice for which the energy profile is shown in Fig. 6. Near the interfaces between object and air, the number of hits is clearly increased, while hits behind the object it are decreased (Fig. 8a). This is due to multiple Coulomb scattering, which occurs only out of the object. As seen in Fig. 8b, a relatively large number of protons enter the front of the object and leave it before reaching the back side, explaining the larger spread of energies close to the edges and the fuzzy edge profile seen in Figs. 5 and 6.

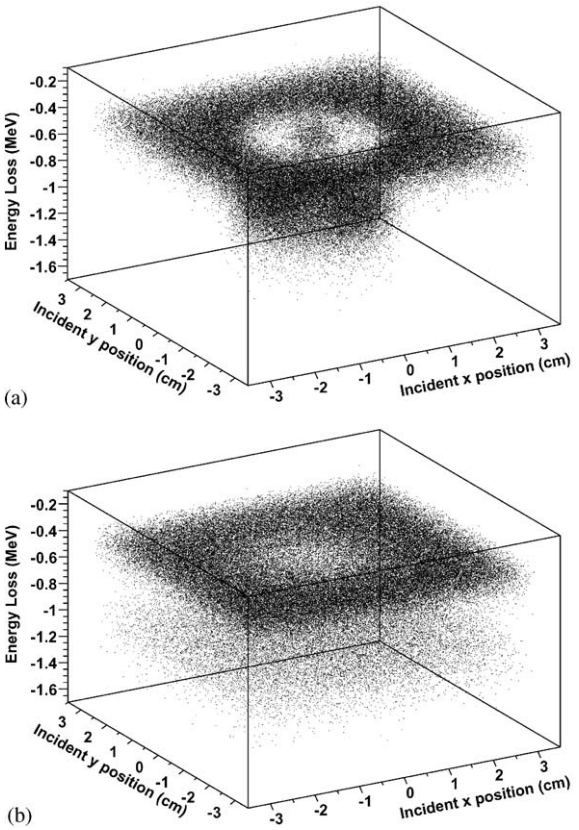

Fig. 7. Monte Carlo simulation of the Si energy-loss distribution in the upstream (top) and downstream (bottom) SSD modules. The "top hat" distribution of the object, clearly visible in the first module, is almost completely washed out in the second module, the result of multiple scattering.

The effect of proton migration on the energy loss spectrum is shown in Fig. 9. Fig. 9a shows the energy loss spectrum for protons by-passing the object, which corresponds to the Landau spectrum expected for the quasi-monoenergetic protons after traversing the wax. In comparison, the spectrum of protons entering the object (Fig 9b) has two components: the first owing to protons that traverse the entire object, and the second due to protons (indicated by open circles in Figs. 8b and 9b) that leave the object before they reach its back surface. The latter, therefore, have higher energy and lower silicon energy loss, which ranges from that of protons entirely missing the object to that of protons traversing the entire object. In

principle, it should be possible to counteract the effects of multiple scattering and beam divergence by measuring the exit angles of individual protons with the silicon telescope and applying appropriate cuts. This possibility will be investigated in future simulations.

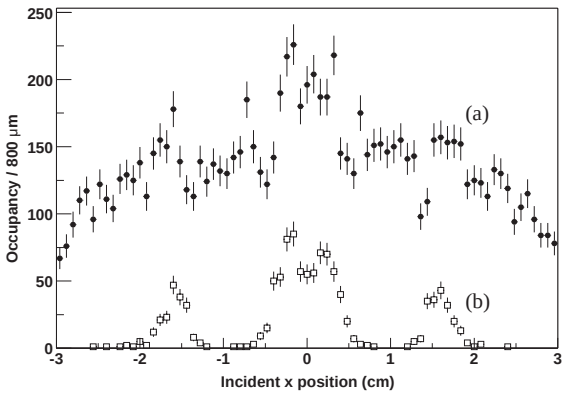

Fig. 8. Monte Carlo simulation of particle migration. Number of hits per four-by-four strip pixel (occupancy) along the central slice: (a) occupancy of all protons and (b) occupancy of protons which enter the front of the object and exit through its sides. The migration from the inside interface into the center and from the outside interface into the periphery lead to the fuzzy edges of the energy-loss profile and the large RMS observed at these locations in Fig. 6.

7. Conclusions

The exploratory data show that imaging with protons based on energy-loss measurement in silicon is possible. In addition the simulations with the GEANT4 program describe the features of the images well, e.g., the influence of multiple scattering and proton migration on the energy and position resolution.

In continuation of our project, we will investigate the following issues:

Improvement of the spatial resolution with a cut on the exit angle: In the analysis described, the object images appeared fuzzy owing to proton migration associated with large exit angles. In the next step, the correlation between the exit angle and the energy will be exploited, and appropriate cuts will be applied to sharpen up the images.

Optimization of the initial proton energy as a function of object size and density: In our exploratory study, the selected proton energy was chosen to achieve maximum image contrast. In the future we will balance density resolution and spatial resolution resulting from multiple Coulomb scattering. It is expected that with increasing proton energy, the energy resolution decreases approximately linearly and that spatial resolution improves as multiple scattering decreases inversely.

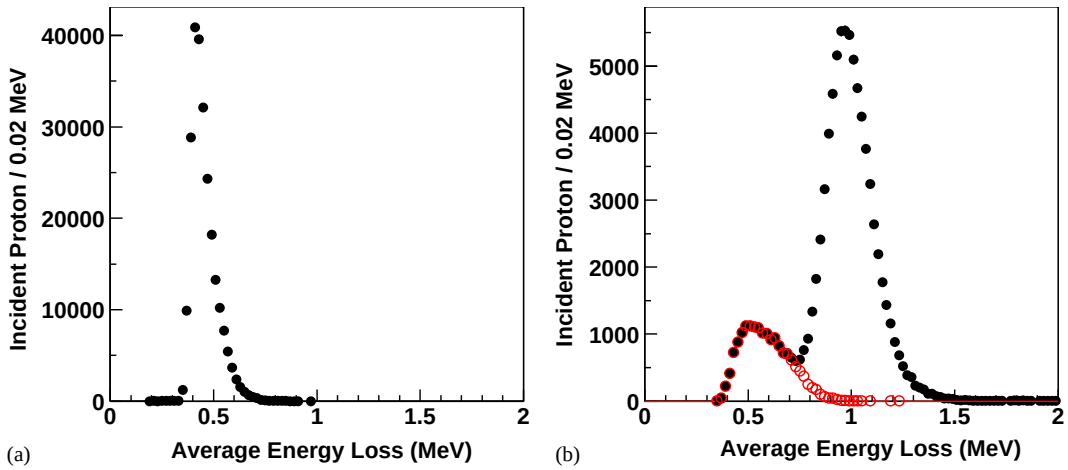

Fig. 9. Monte Carlo simulation of the energy loss spectrum in the first SSD module of the protons missing the object (a) and the protons entering the object (b). The open circles correspond to the energy loss of migrating protons, entering the object but exiting through its sides. The shift of the main peak in Fig. 9b toward a larger energy loss is explained by the fact that protons completely traversing the object have significantly lower energies.

Thus, an optimal entrance energy may be chosen depending on size and density of the object and which feature of the image needs to be optimized.

Exploration of the dose–resolution relationship: Imaging with protons as presented here is based on the energy loss of individual particles in the object. The image contrast (energy resolution) and the spatial resolution depend on the number of particles traversing the object and the tightness of the cuts on the data. Thus, image contrast and resolution can be evaluated as functions of the dose to the object, which is of concern for medical applications of PCT and PTR.

Investigation of other methods of energy measurement: The energy resolution in the silicon detectors is of the order 20% in the 100–200 MeV energy range, which could mean that the image contrast at acceptable dose levels is insufficient. Therefore, other techniques of energy measurement independent from the silicon detectors, which would still be used for particle tracking, will be explored.

Acknowledgements

This work was supported by Calspace and the National Medical Technology Testbed Inc. (NMTB) under the US Department of the Army Medical Research Acquisition Activity, Cooperative Agreement Number DAMD17-972-7016. The views and conclusions contained in this presentation are those of the authors and do not necessarily reflect the position or the policy of the US Army or NMTB.

We thank Bill Rowe and Alec Webster for valuable technical assistance. H.F.-W.S. thanks the organizers of RESMDD02 for a stimulating and enjoyable conference.

References

[1] J.M. Slater, J.O. Archambeau, D.W. Miller, M.I. Notarus, W. Preston, J.D. Slater, Int. J. Radiat. Oncol. Biol. Phys. 22 (1992) 383.
[2] U. Schneider, E. Pedroni, Med. Phys. 22 (1995) 353.
[3] H. Bichsel, Passage of Charged Particles Through Matter, American Institute of Physics Handbook, McGraw-Hill, New York, 1972, pp. 8-142–8-189.
[4] D.E. Groom (Ed.), Review of Particle Physics, Eur. Phys. J. C15, (2000) pp. 1–878.
[5] National Institute for Standards and Technology, PSTAR database, http://physics.nist.gov/PhysRefData/Star/Text/PSTAR.html.
[6] B. Keeney, V. Bashkirov, R.P. Johnson, W. Kroeger, H. Ohyama, et al., IEEE Trans. Nucl. Sci. NS-49 (2002) 1724.
[7] E. do Couto e Silva, G. Godfrey, P. Anthony, R. Arnold, H. Arrighi, et al., Nucl. Instr. and Meth. 474 (1) (2001) 19.
[8] R.P. Johnson, P. Poplevin, H.F.-W. Sadrozinski, E. Spencer, IEEE Trans. Nucl. Sci. NS-45 (1998) 927.
[9] GEANT4 Workshop at SLAC, February 18–22, 2002, http://geant4.slac.stanford.edu/UsersWorkshop/.